Inorg. Chem. **2007**, *46*, 4187−4196

Dimerization Processes of Square Planar $[Pt^{II}(^tbpy)(dithiolato^{\bullet})]^+$ Radicals

József Sándor Pap,[†] Flávio Luiz Benedito,[†] Eberhard Bothe,[†] Eckhard Bill,[†] Serena DeBeer George,[‡] Thomas Weyhermüller,[†] and Karl Wieghardt*[,†]

Max-Planck-Institut für Bioanorganische Chemie, Stiftstrasse 34-36, D-45470 Mülheim an der Ruhr, Germany, and Stanford Synchroton Radiation Laboratory, SLAC, Stanford University, Stanford, California 94309

Received January 25, 2007

The preparation and structural characterization of the neutral, square planar complexes $[Pt^{II}(^tbpy)(A)]$ (**1**), $[Pt^{II}(^tbpy)(B)]$ (**2**), and $[Pt^{II}(PPh_3)_2(B)]$ (**3**) have been accomplished, where (^{t}bpy) = 4,4′-di-*tert*-butylpyridine, $(A)^{2-}$ = 3,6-bis(trimethylsilyl)-1,2-benzenedithiolate(2–), and $(B)^{2-}$ = 1,2-bis(4-*tert*-butylphenyl)ethylene-1,2-dithiolate(2–) and $(A^{\bullet})^{1-}$ and $(B^{\bullet})^{1-}$ represent the corresponding monoanionic radicals. Electrochemical and chemical one-electron oxidation of **1** and **2** in CH_2Cl_2 solution affords the monomeric monocations $[Pt^{II}(^tbpy)(A^{\bullet})]^+$ (**1a**) and $[Pt^{II}(^tbpy)(B^{\bullet})]^+$ (**2a**), both of which possess an $S = {}^1/_2$ ground state. The corresponding spin doublet monocationic dimers $[Pt^{II}_2(^tbpy)_2(A)(A^{\bullet})]^+$ (**1b**) and $[Pt^{II}_2(^tbpy)_2(B)(B^{\bullet})]^+$ (**2b**) were electrochemically generated in solution (50% oxidation) and identified by X-band EPR spectroscopy. Complete one-electron oxidation of **1** and **2** yielded the diamagnetic dimers $[Pt^{II}_2(^tbpy)_2(A^{\bullet})_2]^{2+}$ (**1c**) and $[Pt^{II}_2(^tbpy)_2(B^{\bullet})_2]^{2+}$ (**2c**) which are in equilibrium with the corresponding paramagnetic monomers **1a** and **2a** in solution. The crystal structure of $[Pt^{II}_2(^tbpy)_2(B^{\bullet})_2](PF_6)_2\cdot 3CH_2Cl_2$ (**2c**) revealed a centrosymmetric, lateral dimer whose bridging part is a $Pt^{II}_2(\mu_2\text{-}S)_2$ rhomb; the metal ions possess a square based pyramidal geometry. Solid-state sulfur K-edge X-ray absorption spectra of **1**, **2**, **2a**, **2c**, and $[Pt^{II}(B^{\bullet})_2]^0$ (**4**) have been recorded, which clearly show that a sulfur-centered radical $(B^{\bullet})^{1-}$ is present in **2a**, **2c**, and **4**. The absence of ligand-based radicals in **1** and **2** is also clearly established. One-electron oxidation of $[Pt(PPh_3)_2(B)]$ (**3**) afforded only the spin doublet species $[Pt^{II}(PPh_3)_2(B^{\bullet})]^+$ (**3a**); no dimer formation was detected. Synthesis and crystal structure of square planar $[Pt^{II}(B^{\bullet})_2]^0\cdot$thf are also reported.

Introduction

Square planar $[Pt^{II}(diimine)(dithiolato)]^0$ complexes are known to possess unique photophysical properties.[1] Many such complexes have been prepared by using a diimine-type ligand such as 2,2′-bipyridine,[2−4] biacetylbis(anil),[5] and 1,-10-phenanthroline[6] (and their substituted derivatives[1,7−10]) and a dithiolate ligand such as 1,2-benzenedithiolates-(2−)[3−5,10−12] and 1,1-dithiolates(1−)[7,8,13] or heterocyclic ligands with a dithiolate chelating functional group[1,14−16]

* To whom correspondence should be addressed. E-mail: wieghardt@mpi-muelheim.mpg.de.
[†] Max-Planck-Institut für Bioanorganische Chemie.
[‡] Stanford University.

(1) (a) Paw, W.; Cummings, S. D.; Mansour, M. A.; Connick, W. B.; Geiger, D. K.; Eisenberg, R. *Coord. Chem. Rev.* **1998**, *171*, 125−150. (b) Cummings, S. D.; Eisenberg, R. *Prog. Inorg. Chem.* **2004**, *52*, 315.
(2) Vogler, A.; Kunkely, H. *J. Am. Chem. Soc.* **1981**, *103*, 1559−1660.
(3) Puthraya, K. H.; Srivastava, T. S. *Tetrahedron* **1985**, *4*, 1579−1584.
(4) Connick, W. B.; Gray, H. B. *J. Am. Chem. Soc.* **1997**, *119*, 11620−11627.
(5) Vogler, A.; Kunkely, H.; Hlavatsch, J.; Merz, A. *Inorg. Chem.* **1984**, *23*, 506−509.
(6) Zuleta, J. A.; Burberry, M. S.; Eisenberg, R. *Coord. Chem. Rev.* **1990**, *97*, 47−64.
(7) Zuleta, J. A.; Chesta, C. A.; Eisenberg, R. *J. Am. Chem. Soc.* **1989**, *111*, 8916−8917.
(8) Zuleta, J. A.; Bevilacqua, J. M.; Rehm, J. M.; Eisenberg, R. *Inorg. Chem.* **1992**, *31*, 1332−1337.
(9) Geary, E. M. A.; Yellowlees, L. J.; Jack, L. A.; Oswald, I. D. H.; Parsons, S.; Hirata, N.; Durrant, J. R.; Robertson, N. *Inorg. Chem.* **2005**, *44*, 242−250.
(10) Weinstein, J. A.; Tierney, M. T.; Davies, E. S.; Base, K.; Robeiro, A. A.; Grinstaff, M. W. *Inorg. Chem.* **2006**, *45*, 4544−4555.
(11) Makedonas, C.; Mitsopoulou, C. A.; Lahoz, F. J.; Balana, A. I. *Inorg. Chem.* **2003**, *42*, 8853−8865.
(12) Gosh, P.; Begum, A.; Herebian, D.; Bothe, E.; Hildenbrand, K.; Weyhermüller, T.; Wieghardt, K. *Angew. Chem., Int. Ed.* **2003**, *42*, 563−567.
(13) Bevilacqua, J. M.; Eisenberg, R. *Inorg. Chem.* **1994**, *33*, 2913−2923.
(14) Smucker, B. W.; Hudson, J. M.; Omary, M. A.; Dunbar, K. R. *Inorg. Chem.* **2003**, *42*, 4714−4723.

10.1021/ic070130+ CCC: $37.00
Published on Web 04/12/2007

and 1,2-ethylenedithiolate(2−) derivatives.[1,5,9,13] All of these species display an intense solvatochromic absorption band in the visible region, which has been assigned[17] as a charge-transfer transition from a filled orbital of mixed Pt d and dithiolate p composition (HOMO) to the lowest unoccupied molecular orbital (LUMO). The LUMO is predominantly π^* diimine character, which was proven by EPR and ENDOR spectroscopy in conjunction with DFT calculations[19] for the one-electron reduced form $[Pt^{II}(diimine^{\bullet})(L)_2]^-$ (diimine = bpy; $(diimine^{\bullet})^{1-}$ is the corresponding radical anion; L = Cl^-, CN^-). Extended Hückel[16,30] and more recent DFT calculations[11] indicate that the HOMO in the neutral complex is predominantly dithiolate sulfur 3p with some metal 5d contribution (∼14%) in character.

According to these orbital properties, the absorption of visible light by [Pt^{II}(diimine)(dithiolate)] complexes leads to a triplet excited state in which one electron from the donating dithiolate dominated HOMO is excited to the acceptor LUMO, i.e., π^* orbital of the diimine ligand (it is noted that in several cases there are multiple emitting states,[13] including a diimine $\pi-\pi^*$ intraligand state). The excitation energy can be transmitted by emitting light, which causes solution-luminescence of these species, or by self-quenching reactions, which occur via excited state/ground state Pt···Pt interactions.[21] Also, in the presence of reductive or oxidative quenching molecules, the corresponding ground state $[Pt^{II}(diimine^{\bullet})(dithiolate)]^-$ or $[Pt^{II}(diimine)(dithiolate^{\bullet})]^+$ can be formed via a photoinduced electron-transfer reaction.[1] Several complexes were also found to undergo photoinduced reactions in the presence of molecular oxygen, where the reaction involves addition of oxygen to the sulfur of the complexed dithiolate.[4,22,23] The fundamental basis for the photoinduced electron-transfer reactions of these [Pt^{II}(diimine)(dithiolate)] complexes is that both the diimine-type ligands and the dithiolates are redox-active. The redox-activity of coordination dithiolate ligands is well established by spectroscopic studies (IR, RR, X-ray, EPR, sulfur K-edge XAS) and theoretical (correlated ab initio and density functional) calculations[24−26] carried out recently on $[M(L)_2]^z$ complexes (M = Ni^{II}, Pd^{II}, Pt^{II}, Cu^{III}, Au^{III}; $z = 1+ \rightarrow 2-$; L = 1,2-benzenedithiolate or 1,2-disubstituted 1,2-ethylene-dithiolate ligands).

Chart 1

Ligands

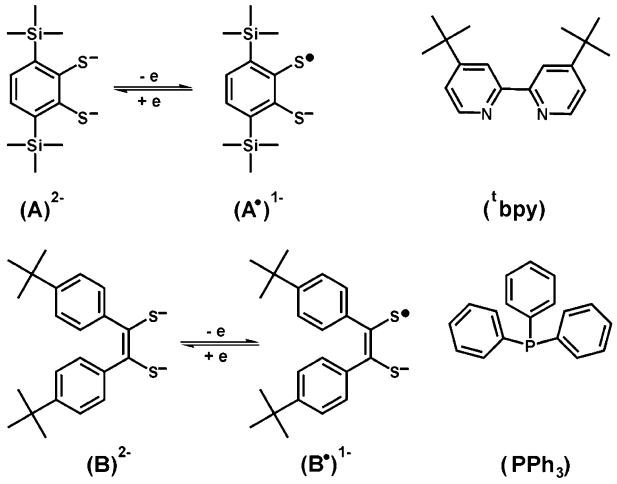

Complexes

$[Pt^{II}(^tbpy)(A)]^0$	**1**	$[Pt_2^{II}(^tbpy)_2(B^{\bullet})_2](PF_6)_2$	**2c**
$[Pt^{II}(^tbpy)(B)]^0$	**2**	$[Pt^{II}(B^{\bullet})_2]$	**4**
$[Pt^{II}(PPh_3)_2(B)]^0$	**3**		

In contrast, the one-electron oxidized form $[Pt^{II}(diimine)(dithiolato^{\bullet})]^+$ containing a dithiolate(1−) ligand radical has not been isolated as a stable salt to date. Only the EPR spectrum of an electrochemically generated species, $[Pd^{II}(bpy)(C^{\bullet})]^+$, has been reported in frozen CH_2Cl_2 solution where $(C^{\bullet})^{1-}$ is the monoanionic π radical form of 4,6-di-*tert*-butyl-benzene-1,2-dithiolate(2−).[12] This species was proposed to rapidly dimerize in liquid solution affording a diamagnetic dimer which was found to be EPR silent. A similar radical species has recently been generated in solution, namely, $[Pt^{II}(dpphen)(C^{\bullet})]^+$, and its EPR spectrum has also been reported.[10]

In this Article we describe the preparation and full characterization of the mononuclear neutral complexes [Pt^{II}(^{t}bpy)(A)] (**1**) and [Pt^{II}(^{t}bpy)(B)] (**2**) (^{t}bpy = 4,4′-di-*tert*-butylbipyridine, $(A)^{2-}$ = 3,6-bis(trimethylsilyl)benzene-1,2-dithiolate(2−), and $(B)^{2-}$ = 1,2-bis(4-*tert*-butylphenyl)ethylene-1,2-dithiolate(2−)) as shown in Chart 1. The electrochemical oxidations of these species revealed the presence of dimerization processes affording dinuclear monocationic paramagnetic intermediates and diamagnetic dicationic dimers. $[Pt^{II}_2(^tbpy)_2(B^{\bullet})_2](PF_6)_2$ (**2c**) has been isolated in crystalline form. Its crystal structure provides the first example of a mixed-ligand, dithiolate(1−) π radical containing complex.

In contrast, the square planar analogue $[Pt^{II}(PPh_3)_2(B)]$, which has also been prepared, remains mononuclear upon

(15) Nakahama, A.; Nakamo, M.; Matsubayashi, G.-E. *Inorg. Chim. Acta* **1999**, *284*, 55−60.
(16) Matsubayashi, G.-E.; Hirao, M.; Tanaka, T. *Inorg. Chim. Acta* **1988**, *144*, 217−221.
(17) Zuleta, J. A.; Bevilacqua, J. M.; Prosperpio, D. M.; Harvey, P. D.; Eisenberg, R. *Inorg. Chem.* **1992**, *31*, 2396−2404.
(18) Cummings, S. D.; Eisenberg, R. *J. Am. Chem. Soc.* **1996**, *118*, 1949−1960.
(19) McInnes, E. J. L.; Farley, R. D.; Macgregor, S. A.; Taylor, K. J.; Yellowlees, L. J.; Rowlands, C. C. *J. Chem. Soc., Faraday Trans.* **1998**, *94*, 2985−2991.
(20) Benedix, R.; Hennig, H. *Inorg. Chim. Acta* **1988**, *141*, 21−26.
(21) Connick, W. B.; Geiger, D.; Eisenberg, R. *Inorg. Chem.* **1999**, *38*, 3264−3265.
(22) Shukla, S.; Kamath, S. S.; Srivastava, T. S. *J. Photochem. Photobiol., A* **1989**, *50*, 199−207.
(23) Zhang, Y.; Ley, K. D.; Schanze, K. S. *Inorg. Chem.* **1996**, *35*, 7102−7110.
(24) Ray, K.; Weyhermüller, T.; Neese, F.; Wieghardt, K. *Inorg. Chem.* **2005**, *44*, 5345−5360.
(25) Ray, K.; Weyhermüller, T.; Goosens, A.; Crajé, M. W. J.; Wieghardt, K. *Inorg. Chem.* **2003**, *42*, 4082−4086.
(26) Szilágyi, R. K.; Lim, B. S.; Glaser, T.; Holm, R. H.; Hedman, B.; Hodgson, K. O.; Solomon, E. I. *J. Am. Chem. Soc.* **2003**, *125*, 9158−9169.
(27) Beswick, C. L.; Schulman, J. M.; Stiefel, E. I. In *Dithiolene Chemistry: Synthesis, Properties, and Applications*; Stiefel, E. I., Karlin, K. D., Eds.; Progress in Inorganic Chemistry, Vol. 52; John Wiley & Sons, Inc.,: Hoboken, NJ, 2004; pp 73−76.

Table 1. Crystallographic Data for **1**, **2c**·3CH_2Cl_2, **3**·3$CHCl_3$, and **4**·Toluene

	1	**2c**·3CH_2Cl_2	**3**·3$CHCl_3$	**4**·toluene
chemical formula	$C_{30}H_{44}N_2PtS_2Si_2$	$C_{83}H_{106}Cl_6F_{12}N_4P_2Pt_2S_4$	$C_{61}H_{59}Cl_9P_2PtS_2$	$C_{51}H_{60}PtS_4$
fw	748.06	2180.78	1432.28	996.32
space group	$P2_1/c$ (No. 14)	$P2_1/n$ (No. 14)	$P\bar{1}$ (No. 2)	$Pna2(1)$ (No. 33)
a, Å	15.2157(4)	10.8207(3)	11.7310(6)	11.9920(8)
b, Å	11.1370(4)	21.3485(6)	13.7027(7)	35.632(2)
c, Å	19.9789(6)	20.2643(6)	20.5167(12)	11.1812(6)
α, deg	90	90	103.082(4)	90
β, deg	106.995(3)	97.130(3)	105.661(4)	90
γ, deg	90	90	96.134(4)	90
V, Å^3	3237.7(2)	4645.0(2)	3043.1(3)	4777.7(5)
Z	4	2	2	4
T, K	100(2)	100(2)	100(2)	100(2)
ρ_{calcd}, g cm^{-3}	1.535	1.559	1.563	1.385
reflns collected/$2\theta_{max}$	87925/70.0	72493/62.0	31494/55.0	41461/51.9
unique reflns/$I > 2\sigma(I)$	14241/12619	14772/12699	13913/12554	8615/6663
no. of params/restrictions	346/0	557/28	682/0	479/1
μ, cm^{-1}/λ, Å	45.58/0.71073	33.73/0.71073	28.60/0.71073	31.44/0.71073
R1[a]/goodness of fit[b]	0.0275/1.105	0.0298/1.035	0.0512/1.102	0.0525/1.011
wR2[c] ($I > 2\sigma(I)$)	0.0527	0.0602	0.1269	0.1198
residual density, e Å^{-3}	+1.235/−1.389	+1.286/−1.024	+3.792/−2.402	3.09/−1.83

[a] Observation criterion: $I > 2\sigma(I)$. R1 = $\sum||F_o| - |F_c||/\sum|F_o|$. [b] GOF = $[\sum[w(F_o^2 - F_c^2)^2]/(n-p)]^{1/2}$. [c] wR2 = $[\sum[w(F_o^2 - F_c^2)^2]/\sum[w(F_o^2)^2]]^{1/2}$ where $w = 1/\sigma^2(F_o^2) + (aP)^2 + bP$ and $P = (F_o^2 + 2F_c^2)/3$.

Table 2. Selected Bond Distances (Å) and Angles (deg) for **1**, **2c**, **3**, and **4**

			1		
Pt(1)−N(21)	2.0513(16)	S(1)−C(1)	1.7604(19)	N(21)−Pt(1)−N(32)	78.74(6)
Pt(1)−N(32)	2.0605(15)	S(2)−C(2)	1.7664(18)	S(1)−Pt(1)−S(2)	88.19(2)
Pt(1)−S(1)	2.2461(5)	C(1)−C(2)	1.411(3)	N(32)−Pt(1)−S(1)	174.80(5)
Pt(1)−S(2)	2.2430(5)			N(21)−Pt(1)−S(2)	175.49(4)
			2c		
Pt(1)−N(42)	2.0519(19)	S(1)−C(1)	1.723(2)	N(31)−Pt(1)−N(42)	79.07(8)
Pt(1)−N(31)	2.0649(19)	S(2)−C(2)	1.717(2)	S(1)−Pt(1)−S(2)	87.44(2)
Pt(1)−S(1)	2.2432(6)	C(1)−C(2)	1.387(3)	N(31)−Pt(1)−S(2)	162.77(6)
Pt(1)−S(2)	2.2304(6)	Pt(1)−S(1a)	2.8619(6)	N(42)−Pt(1)−S(1)	174.47(6)
		Pt(1a)−S(1)	2.8618(6)		
			3		
Pt(1)−P(50)	2.2829(14)	S(1)−C(1)	1.764(5)	P(30)−Pt(1)−P(50)	98.70(5)
Pt(1)−P(30)	2.3004(13)	S(2)−C(2)	1.771(6)	S(1)−Pt(1)−S(2)	87.02(5)
Pt(1)−S(1)	2.3036(14)	C(1)−C(2)	1.354(8)	P(30)−Pt(1)−S(2)	168.92(5)
Pt(1)−S(2)	2.3034(12)			P(50)−Pt(1)−S(1)	173.73(5)
			4		
Pt(1)−S(1)	2.243(2)	S(1)−C(1)	1.728(9)	C(1)−C(2)	1.381(12)
Pt(1)−S(2)	2.242(2)	S(2)−C(2)	1.729(8)	C(31)−C(32)	1.404(13)
Pt(1)−S(31)	2.259(2)	S(31)−C(31)	1.709(10)		
Pt(1)−S(32)	2.243(2)	S(32)−C(32)	1.685(9)		

oxidation to [Pt^{II}(PPh$_3$)$_2$(B$^{\bullet}$)]$^+$. Its EPR spectrum has been investigated.

Finally, the homoleptic species [Pt^{II}(B$^{\bullet}$)$_2$] (**4**) ($S = 0$) has been synthesized and structurally characterized. In conjunction with the structure of **3**, it has been possible to establish the differing C−S and C−C bond lengths in a closed shell dianion (B)$^{2-}$ vs its one-electron oxidized radical (B$^{\bullet}$)$^{1-}$ form.

Results and Discussion

Syntheses. The disodium salt of the ligand 3,6-bis-(trimethylsilyl)benzene-1,2-dithiol (Chart 1), Na_2[A], has been synthesized by using commercially available 1,2-bis-(isopropylthio)benzene.[28] The isopropyl protecting groups are necessary in order to avoid possible oxidative dimerization processes with concomitant S−S bond formation. Ortholithiation of 1,2-bis(isopropylthio)benzene was achieved with a large excess of *n*-butyllithium in *n*-hexane solution in the presence of *N*,*N*,*N*′,*N*′-tetramethylethylenediamine as the base. Addition of trimethylsilylchloride afforded 1,2-bis-(isopropylthio)-3-trimethylsilylbenzene in excellent yields. Repetition of the above reaction sequence yielded the final product 1,2-bis(isopropylthio)-3,6-bis(trimethylsilyl)benzene. S-Deprotection was carried out at −78 °C in liquid ammonia with elemental sodium[29] affording the extremely air-sensitive salt Na_2[A].

When an acetonitrile solution of [Pt^{II}(^{t}bpy)Cl$_2$] was mixed with 1 equiv of Na_2[A] under an Ar blanketing atmosphere, the solution turned purple and crystalline purple [Pt^{II}(^{t}bpy)-(A)] (**1**) precipitated upon cooling to 0 °C. Similarly, the reaction of [Pt^{II}(^{t}bpy)Cl$_2$] with a cold dioxane solution of the in situ generated thiophosphoric ester[30] of the ligand 1,2-

(28) Sato, R.; Ohyama, T.; Kawagoe, T.; Baba, M.; Nakajo, S.; Kimura, T.; Ogawa, S. *Heterocycles* **2001**, *55* (*1*) 145−154.

(29) Hahn, F. E.; Seidel, W. W. *Angew. Chem., Int. Ed. Engl.* **1995**, *107* (23−24), 2938−2941.

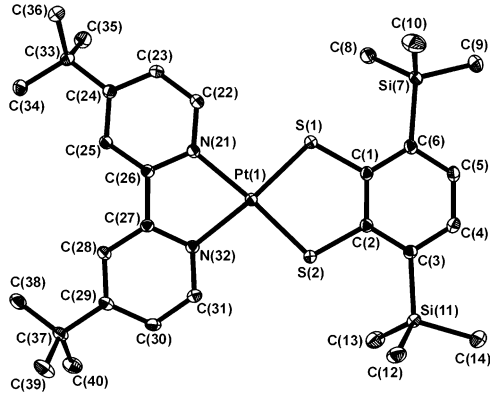

Figure 1. Molecular structure of the neutral complex in crystals of **1** (thermal ellipsoids are drawn at the 50% probability level).

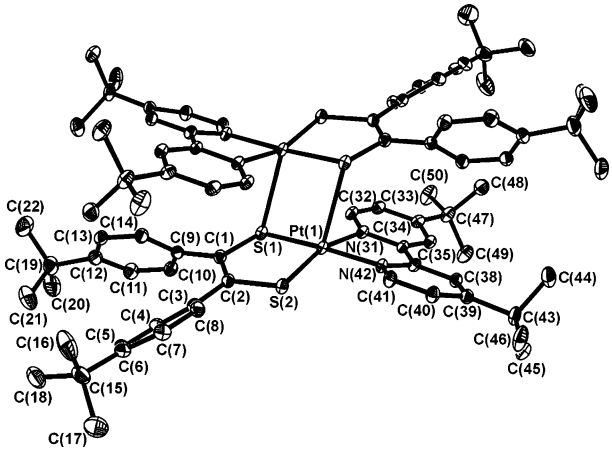

Figure 2. Structure of the dication in crystals of **2c** (thermal ellipsoids are drawn at the 50% probability level).

bis(4-*tert*-butylphenyl)ethylene-1,2-dithiol (H_2[B]) generated crystalline blue [Pt^{II}(^{t}bpy)(B)]^0 (**2**).

When a solution of **2** in CH_2Cl_2 was oxidized under an Ar blanketing atmosphere with 1 equiv of ferrocenium hexafluorophosphate, a dimeric dication formed which was isolated as a black hexafluorophosphate salt, [Pt^{II}_2(^{t}bpy)$_2$-($B^{\bullet}$)$_2$](PF_6)$_2$ (**2c**).

The neutral complex [Pt^{II}(PPh_3)$_2$(B)] (**3**) was prepared according to the procedure described in ref 31. Crystals suitable for X-ray crystallography were grown from a $CHCl_3$/*n*-hexane mixture (1:1 vol).

The neutral complex [Pt^{II}($B^{\bullet}$)$_2$]·toluene (**4**) has been prepared in a similar fashion as the recently described palladium analogue.[31b] It is a blue-black diamagnetic solid.

Crystal Structures. The crystal structures of **1**, **2c**·3CH_2Cl_2, **3**·3$CHCl_3$, and **4**·toluene have been determined at 100(2) K. Crystallographic details are given in Table 1, and selected bond lengths and angles are listed in Table 2.

The structure of a neutral molecule in crystals of **1** is shown in Figure 1, whereas those of the neutral complexes in crystals of **3**·3$CHCl_3$ (top) and **4**·toluene (bottom) are displayed in Figure 3. Figure 2 exhibits the dication in crystals of **2c**·3CH_2Cl_2.

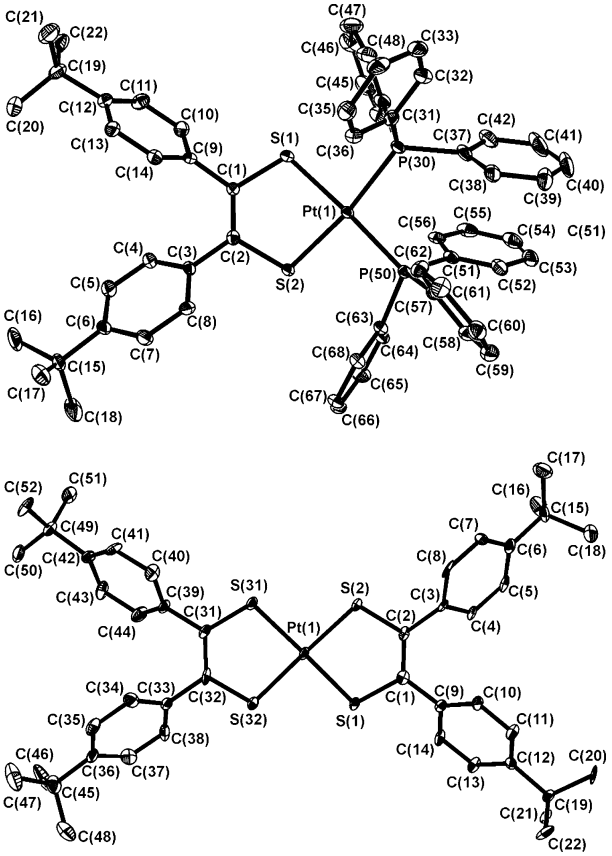

Figure 3. Structure of the neutral molecules in crystals of **3** (top) and **4** (bottom) (thermal ellipsoids are drawn at the 50% probability level).

The neutral complex **1** is nearly square planar; the dihedral angle between the planes S1−Pt1−S2 and N21−Pt1−N32 is only 1.5°. The observed long C−S bond lengths at 1.760(2) and 1.766(2) Å and the nearly equidistant C−C bonds of the dithiolate benzene ring in $(A)^{2-}$ are typical for closed-shell aromatic dithiolate dianions. Similar results have been reported for [M^{II}(bpy)(bdt)] complexes (M = Ni, Pd, Pt)[4] (bdt^{2-} = benzene-1,2-dithiolate) and [Pt^{II}(dpphen)(dtbc)].[10]

The neutral complex **3** (Figure 3) is also square planar. The C−S bonds at 1.764(5) and 1.771(6) Å indicate again the presence of a closed-shell dianion $(B)^{2-}$; the short C1−C2 distance of 1.354(8) Å is in excellent agreement with this notion as it points to considerable C=C double bond character.

The homoleptic neutral molecule in crystals of **4** is shown in Figure 3 (bottom). It is a square planar molecule containing two S,S′-coordinated $(B^{\bullet})^{1-}$ radicals as is clearly deduced from the short av C−S bond length at 1.713 Å and the relatively long av "olefinic" C−C bond distance at 1.393 Å. Thus, the dimensions of a closed shell dianion $(B)^{2-}$ in **3** are clearly different from those of the monoanionic radical $(B^{\bullet})^{1-}$ in **4**.

The most interesting structure of the present series is undoubtedly that of the dinuclear dication shown in Figure 2. It is well established for homoleptic dinuclear complexes containing two bis(dithiolate)metal units that two structure

(30) Schrauzer, G. N.; Mayweg, V. P.; Heinrich, W. *Inorg. Chem.* **1965**, *4*, 1615−1617.

(31) (a) Bowmaker, G. A.; Boyd, P. D. W.; Campbell, G. K. *Inorg. Chem.* **1983**, *22*, 1208−1213. (b) Kokatam, S.-L.; Ray, K.; Pap, J.; Bill, E.; Geiger, W. E.; LeSuer, R. J.; Rieger, P. H.; Weyhermüller, T.; Neese, F.; Wieghardt, K. *Inorg. Chem.* **2007**, *46*, 1100−1111..

types I and II exist, namely, (a) an M−M dimer containing two nearly square planar bis(dithiolene)metal moieties connected by a metal−metal bond or (b) a centrosymmetric lateral M−S dimer with a $M_2(\mu_2\text{-SR})_2$ rhomb in which the metal ion has an irregular five-coordinate geometry. Type II complexes involve often first-row transition metal ions, such as Co, Fe, Ni, whereas for Pt and Pd only type I species have been characterized. For instance, in $[Pt(edt)_2]_2$ (edt = $(S_4C_4H_4^•)^{1-}$, the ethylene-1,2-dithiolate(1−) radical monoanion[32]) the Pt···Pt distance was determined to be 2.748(2) Å and the av Pt−S bond length is 2.300 Å. In $[Pt(dmit)_2]_3$·TTF (TTF = tetrathiafulvalene, H_2(dmit) = 4,5-dimercapto-1,3-dithiol-2-thione), which contains an M−M dinuclear neutral species and a mononuclear species, the Pt···Pt distance is 2.935 Å, whereas the Pt−S bond length is 2.315 Å.[33]

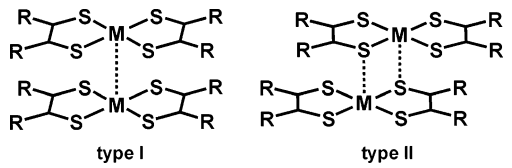

Clearly, the structure of the dication in crystals of **2c** is of type II.

It is quite revealing to compare the bond distances of the dithiolate moieties of the approximately square planar [Pt(^{t}bpy)(B$^•$)]$^{1+}$ building block in the dimer **2c** with those of the neutral mononuclear unit [Pt(PPh_3)$_2$(B)] in crystals of **3**. The C−S and the "olefinic" C−C bond lengths of the dithiolene ligand differ significantly. In neutral **3**, a closed shell dianion [S_2C_2(*p*-*tert*-butylphenyl)$_2$]$^{2-}$ is coordinated to a Pt^{II} center, whereas in **2c** the significantly shorter C−S bonds and the elongated C1−C2 bond indicate the presence of a monoanionic π radical (B$^•$)$^{1-}$. The radical ligand has also been characterized by X-ray crystallography in mononuclear [Pd^{II}(B$^•$)$_2$];[31b] the C−S and C1−C2 bonds are within experimental error and identical with those found here in the dication of **2c**. It is noteworthy that the geometry of the Pt^{II}(^{t}bpy) part in **2c** and in mononuclear **1** are identical within experimental error. In other words, the one-electron oxidation of **2** to **2c** is a ligand centered process where (B)$^{2-}$ is oxidized to the radical (B$^•$)$^{1-}$. The radical [Pt^{II}(^{t}bpy)(B$^•$)]$^{1+}$ ($S = ^1/_2$) dimerizes in solution with generation of the dication in **2c**. As has been shown previously, the dithiolene monoanions are S-centered radicals where the spin density is predominantly localized in a 3p orbital of the sulfur atoms. The bridging Pt···S bonds in the dication are very weak (av 2.862(1) Å) and may best be described as a two center−three electron bond between a half-filled 3p orbital at the sulfur and a filled $5d_{z^2}$ orbital at the Pt(II) center. The spins of the two singularly occupied molecular orbitals (SOMOs) may then couple intramolecularly yielding the observed diamagnetic ground state. The [Pt^{II}(^{t}bpy)(B$^•$)]$^+$ part in the dimeric dication is not quite planar; the N−Pt−N and S−Pt−S planes exhibit a dihedral angle of 16.5°, which is probably due to its dimerization.

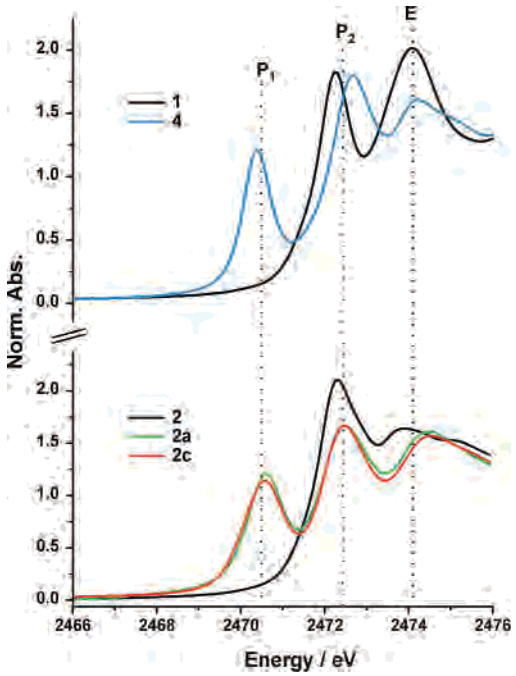

Figure 4. Sulfur K-edge XAS spectra of **1** and **4** (top) and **2**, **2a**, and **2c** (bottom).

Sulfur K-Edge X-ray Absorption Spectra (XAS). Figure 4 shows the normalized sulfur K-edge X-ray absorption spectral (XAS) data for compounds **1**, **2**, **2c**, and **4** (measured as solids) and **2a** (measured as CH_2Cl_2 solution at 25 °C).

The pre-edge features (marked P_1 and P_2 in Figure 4) correspond to transitions to unoccupied antibonding orbitals with sulfur 3p character. The rising edge (marked E) corresponds to a sulfur 1s to 4p transition, the energy of which reflects the effective nuclear charge on the sulfur. Complexes **1** and **2** exhibit an intense single pre-edge feature at ∼2472 eV. In the case of the singlet diradical compound [Pt^{II}(B$^•$)$_2$], an additional pre-edge feature (P_1) appears at lower energy (∼2470 eV), which is consistent with the formation of a ligand-based radical.[34] This assignment is further supported by the increase in the rising edge energy (E), which indicates that the sulfur is more oxidized. Similar changes are observed for complex **2c**, which indicate that a ligand-based oxidation has also occurred. The similarity between the dimer (**2c**) and the monomer (**2a**) in CH_2Cl_2 solution indicates that dimer formation does not significantly perturb the sulfur radical character and thus supports a very weak Pt···S dimer interaction in accordance with the crystal structure.

The absence of a P_1 pre-edge peak in the spectra of **1** and **2** indicates the closed-shell dianionic character of the dithiolate(2−) ligands (A)$^{2-}$ and (B)$^{2-}$.

Electrochemistry. Figure 5 shows the cyclic voltammograms of **1**−**3** in CH_2Cl_2 (0.10 M [N(*n*-Bu)$_4$]PF_6 supporting electrolyte) at 20 °C. The redox potentials are referenced

(32) Browall, K. W.; Bursh, T.; Interrante, L. V.; Kasper, J. S. *Inorg. Chem.* **1972**, *11*, 1800.
(33) Bousseau, M.; Valade, L.; Legros, J.-P.; Cassoux, P.; Garbauskas, M.; Interrante, L. V. *J. Am. Chem. Soc.* **1986**, *108*, 1908.
(34) Ray, K.; DeBeer George, S.; Solomon, E. I.; Wieghardt, K.; Neese, F. *Chem.—Eur. J.* **2007**, *13*, 2753.

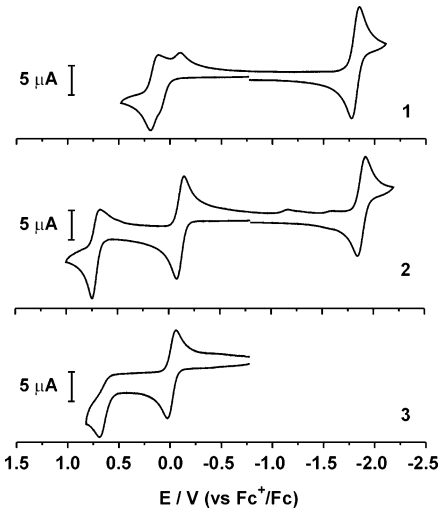

Figure 5. Cyclic voltammograms of **1**−**3** in CH_2Cl_2 (0.10 M $[N(n\text{-}Bu)_4]PF_6$) at a glassy carbon working electrode at 20 °C (scan rate: 200 mV s^{-1}).

versus the ferrocenium/ferrocene couple (Fc^+/Fc) and are listed in Table 3.

Complex **1** displays two successive one-electron redox waves: the first at −1.81 V ($E^1_{1/2}$) is reversible whereas the second ($E^2_{1/2}$) is split into two separate anodic peaks (E^2_{pa} ∼ +0.12 V and $E^{2'}_{pa}$ = +0.19 V) and two cathodic peaks ($E^{2''}_{pc}$ = −0.10 V and $E^{2'}_{pc}$ = 0.11 V). In contrast, the cyclic voltammogram (cv) of **2** exhibits two reversible one-electron-transfer waves at −1.87 V ($E^1_{1/2}$) and −0.10 V ($E^2_{1/2}$) and, in addition, a quasi-reversible one-electron-transfer wave at +0.72 V ($E^3_{1/2}$).

The $E^1_{1/2}$ waves in the cv's of **1** and **2** correspond each to a one-electron reduction of the ^{t}bpy ligand generating a coordinated $(^t\text{bpy}^\bullet)^{1-}$ radical. This process has been described for $[Pt^{II}(bpy)Cl_2]$[19] and for other $[Pt^{II}(bpy)L]$ species (L = benzene-1,2-dithiolate(2−), catecholate, *o*-aminophenolate, and *o*-phenylenediamide).[12,18]

The $E^2_{1/2}$ waves of **1** and **2** are each due to ligand-centered one-electron oxidations of the $(A)^{2-}$ and $(B)^{2-}$ ligands yielding coordinated radicals $(A^\bullet)^{1-}$ and $(B^\bullet)^{1-}$, respectively (Scheme 1). This step yields the monocations $[Pt^{II}(^t\text{bpy})(A^\bullet)]^+$ (**1a**) and $[Pt^{II}(^t\text{bpy})(B^\bullet)]^+$ (**2a**), respectively. The fact that $E^2_{1/2}$ for **1** is actually split into two components indicates that **1a** is not the sole product formed upon electrochemical one-electron oxidation of **1**. As we show below, **1a** and **1** dimerize in solution with formation of the dinuclear species $[Pt^{II}_2(^t\text{bpy})_2(A)(A^\bullet)]^{1+}$ (**1b**) which undergoes a second one-electron oxidation yielding $[Pt^{II}_2(^t\text{bpy})_2(A^\bullet)_2]^{2+}$ (**1c**).

The quasi-reversible oxidation wave $E^3_{1/2}$ for **2** is also believed to be a ligand-centered process in which the neutral 1,2-ethanedithione ligand, $(L^{ox})^0$, is produced. This is a less stable product in solution and probably decomposes on the time scale of a cv measurement where the decomposition products give rise to new peaks at lower potentials (∼ −1.2 and −1.6 V, Figure 5). The dithiolene ligand-based nature of the $E^2_{1/2}$ and $E^3_{1/2}$ redox waves is also nicely corroborated by the cv of **3** in Figure 5 which exhibits a (quasi-)reversible wave at −0.01 V ($E^2_{1/2}$) yielding $[Pt^{II}(PPh_3)_2(B^\bullet)]^+$ (**3a**) and an irreversible oxidation peak at +0.69 V (E^3_{pa}). These values are very similar to those observed for **2** despite the fact that the spectator ligand in **2** is (^{t}bpy) but two triphenylphosphines in **3**.

The coulometric one-electron oxidations of **1**−**3** in CH_2Cl_2 solution containing 0.10 M $[N(n\text{-}Bu)_4]PF_6$ supporting electrolyte have been followed spectroelectrochemically at −25 °C. The results are shown in Figure 6. In each case three electronic spectra have been recorded: (1) the spectrum of the starting complex **1**, **2**, or **3**, (2) the spectrum after 50% of the one-electron oxidation is completed, and (3) the spectrum after 100% of the one-electron oxidation.

The simplest case is that of **3** where a simple transformation **3** → **3a** + e is observed as indicated by the observation of a single, stable isosbestic point at 385 nm (Figure 6, bottom). In the visible range the spectrum after "50% oxidation" is simply that of 50% of the fully oxidized form **3a** since **3** does not absorb in the visible. The fully oxidized species **3a** is paramagnetic and displays an $S = {}^1/_2$ X-band EPR signal (100%) (see below). Thus, **3a** does not dimerize in solution or show indications for the formation of other dinuclear intermediates such as $[Pt^{II}_2(PPh_3)_4(B)(B^\bullet)]^{1+}$ at a 50% oxidation level.

On the other hand, oxidation of **1** in CH_2Cl_2 solution (0.10 M $[N(n\text{-}Bu)_4]PF_6$) displays a much more complex behavior (as does the cv (Figure 6, top)). The spectrum recorded after 50% oxidation exhibits four new absorption maxima at 410, 520, 678, and 861 nm (dashed line in Figure 6). The maximum of **1** at 580 nm has lost half its intensity upon 50% oxidation. On completion of the one-electron oxidation of **1**, a remarkable change of the electronic spectrum occurs (dotted line, Figure 6 top). A significant hypsochromic shift of the two isosbestic points which are present only during the first 50% of the oxidation at 492 and 638 nm is observed. During the completion of the oxidation (50−100%) these isosbestic points are observed at 477 and 605 nm. This is a clear indication that the one-electron oxidation of **1** involves an intermediate. This intermediate is paramagnetic, and from simulations of its EPR spectrum it is concluded that it is a dinuclear species: $[Pt^{II}_2(^t\text{bpy})_2(A)(A^\bullet)]^+$ (**1b**) (see below).

The spectroelectrochemical behavior of the one-electron oxidation of **2** is similar to that of **1** (Figure 6, middle), but clear evidence for **2b** is not readily obtained. A small bathochromic shift of the isosbestic point observed at 530 nm during the first 50% of the oxidation indicates the presence of an intermediate which, as judged from its EPR spectrum (see below), is most probably $[Pt^{II}_2(^t\text{bpy})_2(B)(B^\bullet)]^+$ ($S = {}^1/_2$) (**2b**).

X-Band EPR Spectroscopy. When CH_2Cl_2 solutions containing 0.10 M $[N(n\text{-}Bu)_4]PF_6$ supporting electrolyte and millimolar amounts of **1** or **2** are electrochemically or chemically fully oxidized by one electron at 20 °C, the corresponding frozen solutions are EPR-silent (at T < 80 K) which suggests the exclusive presence of the diamagnetic, dinuclear, dicationic species $[Pt^{II}_2(^t\text{bpy})_2(A^\bullet)_2]^{2+}$ (**1c**) or $[Pt^{II}_2(^t\text{bpy})_2(B^\bullet)_2]^{2+}$ (**2c**), respectively (Figure 2). At 298 K, the EPR spectrum of **2c** in CH_2Cl_2 displays the signal of a spin doublet species with g_{iso} = 2.003 and ^{195}Pt hyperfine

Table 3. Spectroscopic Data and Redox Potentials ($E_{1/2}$ vs Fc^+/Fc) for Complexes

complex	λ, nm (ϵ, M^{-1} cm^{-1})[a]	λ, nm (ϵ, M^{-1} cm^{-1})[a]	$E^1_{1/2}$, V	$E^2_{1/2}$, V	$E^3_{1/2}$, V
1	342 (6000)	580 (8000)	−1.81	*c*	
2	347 (9300)	620 (7600)	−1.87	−0.10	0.72
3	338 (6000)			−0.01	0.69
[Pt(^{t}bpy)(tdt)][b]		563 (7200)	−1.80	−0.01[d]	
[Pt(^{t}bpy)(mnt)][b]		497 (5800)	−1.67	0.54[d]	

[a] In CH_2Cl_2 solution at 20 °C. [b] In dimethylformamide solution, ref 18. Abbreviations: $(tdt)^{2-}$ = 3,4-toluenedithiolate, $(mnt)^{2-}$ = maleonitriledithiolate. [c] Peak potentials (Figure 9): $E^2_{pa} = 0.12$ V; $E^{2\prime}_{pa} = 0.19$ V; $E^{2\prime\prime}_{pc} = -0.10$ V; $E^{2\prime}_{pc} = 0.11$ V. [d] Irreversible; the peak potential is given.

Scheme 1

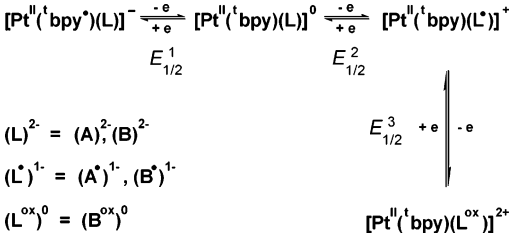

coupling ($I = {}^1/_2$, 33.8%) of 38×10^{-4} cm^{-1} (Figure 7). This signal is due to the mononuclear [Pt^{II}(^{t}bpy)(B$^\bullet$)]$^+$ (**2a**). The intensity of the spectrum (double integral) corresponds to a spin concentration of about 80% of the chemical concentration of the compound. It is thus established that mononuclear **2a** and dinuclear **2c** are in equilibrium in solution. Attempts to detect the corresponding mononuclear radical [Pt^{II}(^{t}bpy)(A$^\bullet$)]$^+$ (**1a**) in solution in a similar fashion failed. Only the dinuclear, EPR silent species **1c** is present in solution at 25 and −90 °C.

Interestingly, electrochemically one-electron oxidized CH_2Cl_2 solutions of **3** display at 10 K a rhombic signal with weak ^{195}Pt hyperfine splitting in its EPR spectrum (Table 4). The signal has been quantitated (100%) and simulated. This signal is due to the presence of mononuclear, paramagnetic [Pt^{II}(PPh$_3$)$_2$(B$^\bullet$)]$^+$ (**3a**). Thus, no dimer formation has been observed in this instance.

In order to find direct evidence for the intermediates of the oxidations of **1** and **2**, we have also carried out stepwise coulometric oxidations of their CH_2Cl_2 (0.10 M [N(*n*-Bu)$_4$]PF$_6$) solutions at −20 °C and recorded their electronic spectra and measured and quantified the corresponding EPR spectra at 30 K. Spin concentrations were obtained by double integration of the EPR derivative spectra and comparison with the signal of a standard 1 mM Cu^{2+} solution in H_2O (2 M $NaClO_4$, 10 mM HCl) measured at the same conditions.

Figure 8 shows the EPR spectra of a 50% oxidized solution of **1** (top) and **2** (bottom) and their respective simulations. The insets show the increasing intensity of the signal with increasing oxidation level up to 50% (one electron removed per two Pt ions). It decreases then again to be EPR-silent at the 100% oxidation level where at 30 K only the diamagnetic dimers **1c** and **2c** exist. This behavior is excellent evidence that the intermediates **1b** and **2b** are paramagnetic dinuclear species: [Pt$^{II}_2$(^{t}bpy)$_2$(A)(A$^\bullet$)]$^{1+}$ (**1b**) and [Pt$^{II}_2$(^{t}bpy)$_2$(B)(B$^\bullet$)]$^{1+}$ (**2b**). In agreement with this notion a satisfactory simulation of the two spectra in Figure 8 requires hyperfine interaction with two ^{195}Pt nucleii as expected for dimeric molecules with natural abundance of ^{195}Pt (33.8%). Details of the simulation and parameters are given in Figure 8 and

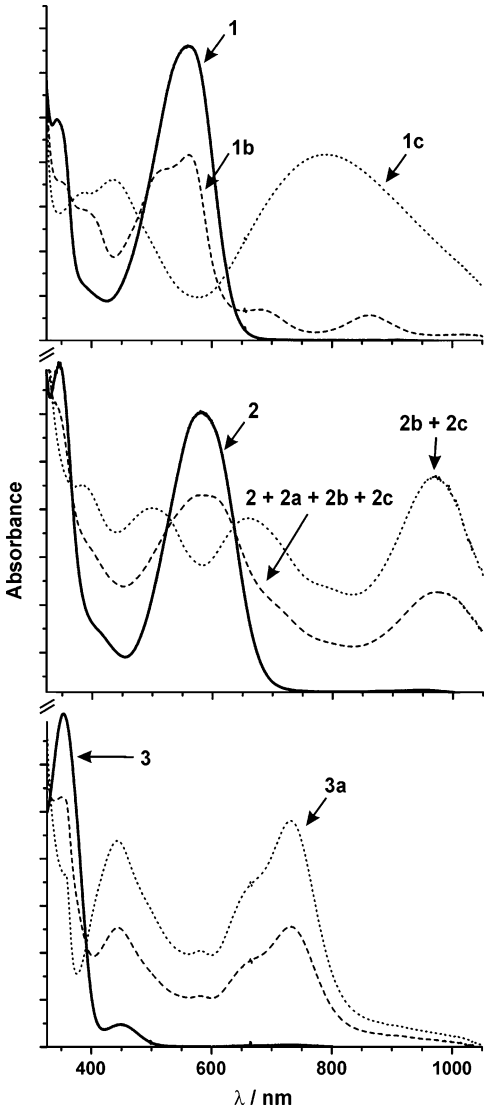

Figure 6. Electronic spectra of **1**−**3** in CH_2Cl_2 solution (0.10 M [N(*n*-Bu)$_4$]PF$_6$) at −25 °C (solid lines). Dashed lines represent the spectra after 50% one-electron oxidation and dotted lines are spectra after 100% oxidation.

Table 4. Within experimental accuracy the ^{195}Pt nuclei appear to be equivalent, which indicates symmetric spin density distribution, either due to strong localization on the bridging sulfur atoms or due to delocalization of the ligand radical. The maximal spin concentration (at 50% electrochemical conversion of the samples) reaches about 50% of the Pt concentration for **1b** but only about 14% for **2b** (see insets of Figure 8). This is due to chemical equilibrium of the singly oxidized dimers (**1b** and **2b**) with nonoxidized and oxidized monomers and doubly oxidized dimers (**1c** and **2c**). Since the concentration of the paramagnetic monomers is negligible

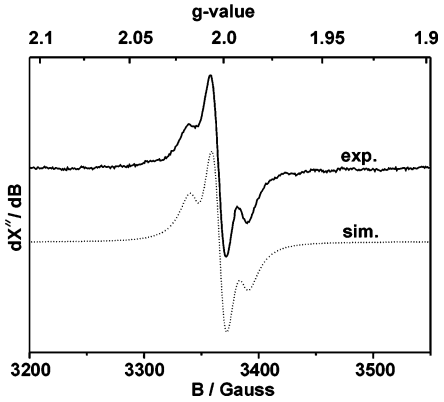

Figure 7. X-band EPR spectrum of chemically ([Fc]PF_6) oxidized **2a** in CH_2Cl_2 solution at 298 K (**2a** is present in 80% based on the spin concentration obtained by double integration; 20% is EPR-silent **2c**). The simulation (dotted line) is the superposition of two isotropic Gaussian spectra with and without hyperfine splitting according to the natural abundance of 33.8% ^{195}Pt nuclei with $I = {}^1/_2$ (see Table 4).

Table 4. X-Band EPR Parameters of $S = {}^1/_2$ Compounds

complex	g_{iso}	g_{xx}	g_{yy}	g_{zz}	^{195}Pt hyperfine coupling constants[d] (10^{-4} cm^{-1})
1b[a]	2.074	2.183	2.167	1.856	$A_{xx} = 200$; $A_{yy} = 153$; $A_{zz} = 140$
2a[b]	2.003				$A_{iso} = 38$[e]
2b[c]	2.061	2.176	2.086	1.914	$A_{xx} = 103$; $A_{yy} = 112$; $A_{zz} = 93$
3a[a]	2.010	2.020	2.006	1.989	$A_{xx} = 70$; $A_{yy} = 20$; $A_{zz} = 90$

[a] In CH_2Cl_2 frozen solution at 10 K. [b] In CH_2Cl_2 solution at 298 K. [c] In CH_2Cl_2 frozen solution at 30 K. [d] The sign of the **A** values is not determined. [e] The value of A_0 measured for **2a** in fluid solution compares well with the anisotropic **A**-tensor components of **2b**, if one assumes that one of the components (presumably A_{zz}) has the opposite sign than the others (which is reasonable if as usual the traceless spin−dipolar contribution is the main source of anisotropy of the **A**-tensor). Then the isotropic part for **2b** can be estimated by $|A_0| = 41 \times 10^{-4}$ cm^{-1}, according to the relation $A_0 = {}^1/_3(A_{xx} + A_{yy} + A_{zz})$.

at low temperatures ($T < 80$ K, see above) and **1c** and **2c** are diamagnetic, the spin concentration of the measured spectra is controlled by the dissociation constants of **1b** and **2b**.

Thus, the spectroelectrochemical results (electronic and EPR spectra) are in agreement with the equilibria shown in Scheme 2. We have not found evidence for the formation of the neutral dinuclear species $[Pt^{II}_2(^t\text{bpy})_2(L)_2]^0$ ($L = (A)^{2-}$, $(B)^{2-}$), and therefore, K_3 must be very small (see below).

Estimation of Equilibrium Constants. With the use of Scheme 2, it has been possible to simulate the current/voltage profiles of the cv's of **1** shown in Figure 9. The shapes of the voltammograms depend mainly on (i) the three equilibrium constants K_{1-3} and the three redox potentials $E^2_{1/2}$, $E^{2'}_{1/2}$, and $E^{2''}_{1/2}$ and (ii) the rate constants for dimerization (k_f, M^{-1} s^{-1}) and dissociation (k_b, s^{-1}) for the three processes in Scheme 2. The six thermodynamic parameters (three K and three $E_{1/2}$) are not completely independent of each other since the sum of the free energy (ΔG^0) values around the two reaction squares in Scheme 2 must add-up to yield zero. The diffusion coefficient was set to 3×10^{-6} cm^2/s for all species involved. The fit parameters are summarized in Table 5. According to the simulation, the chain of events during an anodic scan is one-electron oxidation of **1** to **1a** at E^2_{pa} ($E^2_{1/2}$), followed by a rapid dimerization **1a** + **1** → **1b** and further one-electron oxidation of **1b** to the dinuclear **1c** at $E^{2'}_{pa}$

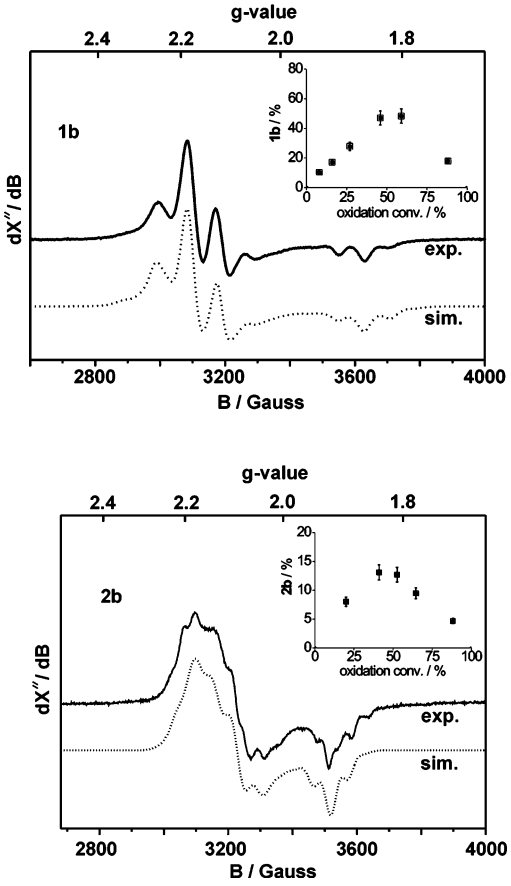

Figure 8. X-band EPR spectra **1b** (top) and **2b** (bottom) in frozen CH_2Cl_2 solution (0.10 M $[N(n\text{-}Bu)_4]PF_6$) at 30 K. Frequency, modulation amplitude, and microwave power for **1b** are 9.4335 GHz, 14 G, and 0.2 mW, respectively, and for **2b** are 9.4213 GHz, 12 G, and 1.0 mW, respectively. The dotted lines are the superposition of three simulated subspectra with Gaussian lines and anisotropic **g** values as given in Table 4 and hyperfine interaction with two, one, and no ^{195}Pt nuclei according to the statistical weights expected for symmetric Pt-dimers with total spin $S = {}^1/_2$ and natural abundance of ^{195}Pt (33.8%): 11.4% double-labeled, 44.8% single labeled, and 43.8% without ^{195}Pt isotope.

Scheme 2

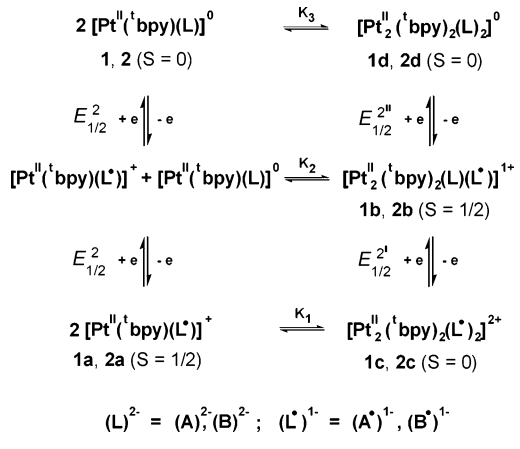

($E^{2'}_{1/2}$). In the cv, the oxidation **1** → **1a** is cathodically shifted because of a kinetic effect of the following equilibrium K_2. Reversing this sequence leads to the reduction **1c** → **1b** at $E^{2'}_{pc}$ ($E^{2'}_{1/2}$) which proceeds at the normal half wave potential $E_{1/2}$ (**1c**/**1b**). Since K_2 is large, the final reduction to **1** takes place at the more negative potential E^2_{pc} via the thermody-

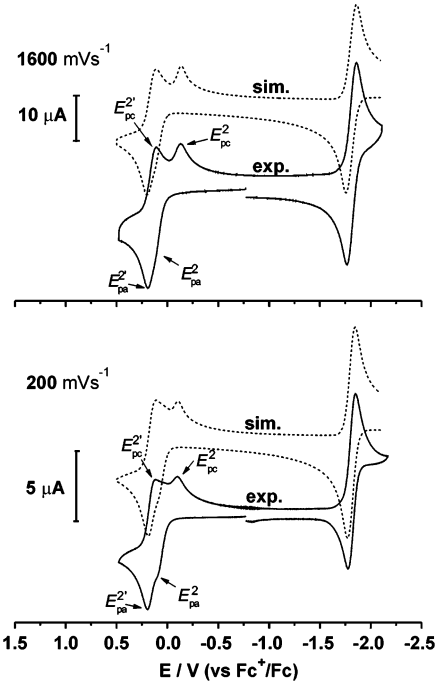

Figure 9. Cyclic voltammogram of **1** in CH_2Cl_2 solution (0.10 M [N(*n*-Bu)$_4$]PF_6) at scan rates 1600 (top) and 200 mV s^{-1} (bottom) at 20 °C and simulations (dotted lines) using parameters given in Table 5.

Table 5. Parameter Set for the Simulation of the Cyclic Voltammogram of **1** (Concentration = 10^{-3} M) at 25 °C ($D = 3 \times 10^{-6}$ cm^2 s^{-1} for All Species)[a]

	K_n, M^{-1}	k_f, M^{-1} s^{-1}	k_b, s^{-1}
K_1	1.31×10^5	2.0×10^8	1.5×10^3
K_2	1.0×10^5	1.2×10^6	0.12×10^3
K_3	~0.5	~10^3	~10^3

[a] Redox potentials vs Fc$^+$/Fc: $E^2{}_{1/2}$, 0.167 V; $E^{2'}{}_{1/2}$, 0.160 V; $E^{2''}{}_{1/2}$, −0.145 V. See Scheme 4.

namically less favorable pathway $E^{2''}{}_{1/2}$ (**1b**/**1d**) with subsequent monomerization to **1**.

Figure 9 shows that the parameter set in Table 5 adequately reproduces the cv of **1** at two different scan rates. Interestingly, at ambient temperature the stability constants for the mono- and dicationic dimers **1b** and **1c** are similar, whereas dimerization of **1** to **1d** is not observed (K_3 is very small) and the redox potentials for the couples **1**/**1a** and **1c**/**1b** are almost identical.

For complex **2**, the equilibrium constant K_1 was determined from UV−vis spectroscopic data. As shown in Figure 10, the electronic spectrum of **2c** in CH_2Cl_2 is strongly temperature dependent in the range from −35 to +33 °C. Concomitantly with the disappearance of the absorption at 685 and 1015 nm, a new absorption maximum grows in at 728 nm upon increasing the temperature from −35 to +33 °C. The process is fully reversible. The low-temperature spectrum is assumed to be that of the dimer **2c**, whereas at 20 °C, mononuclear, paramagnetic **2a** is also present as shown above by EPR spectroscopy (Figure 8).

These observations allow us to assign the spectral changes to the temperature dependence of equilibrium K_1 (see Scheme 2). These K_1 values were calculated by using a molar absorption coefficient of 12 400 M^{-1} cm^{-1} for **2c** at 1015 nm, which was established from a measurement at −50 °C where the dimer **2c** is exclusively present.

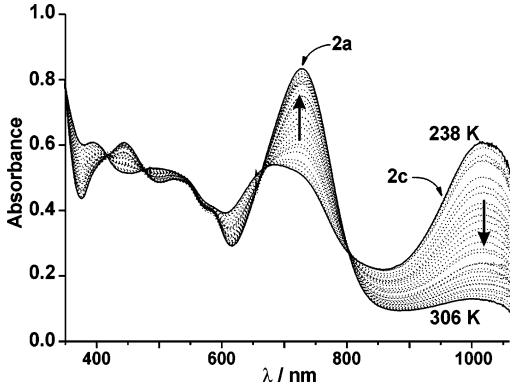

Figure 10. Electronic spectra of **2c** in CH_2Cl_2 solution ($[Pt]_{tot} = 2.44 \times 10^{-4}$ M, $l = 0.5$ cm) recorded in the temperature range from −35 to +33 °C (the arrows represent the direction of the spectral changes).

A value of 660 M^{-1} was found for K_1 of **2c** at 25 °C. From the temperature dependence of K_1 the corresponding enthalpy and entropy values (ΔH^0, ΔS^0 at 295 K) were obtained: $\Delta H^0 = -34 \pm 1$ kJ mol^{-1} and $\Delta S^0 = -59 \pm 2$ J K^{-1} mol^{-1}. Thus, the dimerization reaction is exothermic. Furthermore, the increasing value of K_1 with decreasing temperature (2.3×10^6 M^{-1} is calculated for −90 °C in CH_2Cl_2) indicates that the concentration of paramagnetic **2a** is negligible at −90 °C and therefore not detectable by EPR spectroscopy in frozen solution, in excellent agreement with the EPR experiment at −90 °C.

Experimental Section

Physical Measurements. Electronic spectra of complexes and spectroelectrochemical measurements were recorded on a Hewlett-Packard 8453 spectrophotometer (range 200−1100 nm). Cyclic voltammograms and coulometric measurements were performed with an EG&G potentiostat/galvanostat model 273A. The cyclic voltammetric simulation was carried out with DIGISIM 3.03 from BAS. X-band EPR spectra were recorded on a Bruker ELEXSYS E500 CW-spectrometer equipped with a helium flow cryostat (Oxford Instruments ESR 910) and a Hewlett-Packard frequency counter HP5253B. The EPR spectra were simulated with a self-written program (ESIM, E.B.) for powder spectra from spin $S = {}^1/_2$ systems with anisotropic **g**-tensor and Gaussian or Lorentzian line shape distribution, with an option for automatic parameter optimization. Anisotropic magnetic hyperfine coupling was treated in first-order approximation.

X-ray Crystallographic Data Collection and Refinement of the Structures. A deep purple single crystal of **1**, a black crystal of **2c**, an orange specimen of **3**, and a black specimen of **4** were coated with perfluoropolyether and picked up with glass fibers. The crystals were immediately mounted in the nitrogen cold stream (100 K) of a Nonius Kappa-CCD diffractometer equipped with a Mo-target rotating-anode X-ray source and a graphite monochromator (Mo Kα, $\lambda = 0.710\ 73$ Å). Final cell constants were obtained from least-squares fits of all measured reflections. Crystallographic data of the compounds are listed in Table 1. The Siemens ShelXTL[33] software package was used for solution and artwork of the structure, and ShelXL97[34] was used for the refinement. The structures were readily solved by Patterson methods and subsequent difference Fourier techniques. All non-hydrogen atoms were refined anisotropically. Hydrogen atoms were placed at calculated positions and

refined as riding atoms with isotropic displacement parameters. The PF_6 anion in crystals of **2c** was found to be disordered and was split on two positions in a ratio of about 75:25. Corresponding phosphorus and fluorine atoms of the split positions were refined with equal thermal displacement parameters while P−F distances and F−P−F angles were restrained to be similar. The EADP and SAME instructions of ShelXL97 were used here. A dichloromethane molecule next to a crystallographic inversion center was also disordered. The C−Cl and Cl−Cl distances were restrained using the SADI instruction of ShelXL97, and a fixed occupation factor of 0.5 was assigned. A total of 28 restraints were used for the refinement.

X-ray Absorption Spectroscopy and Measurements and Data Analysis. Sulfur K-edge data were measured at SSRL (under ring conditions of 3.0 GeV and 60−100 mA) using the 54-pole wiggler beam line 6-2 in high magnetic field mode of 10 kG with a Ni-coated harmonic rejection mirror and a fully tuned Si(111) double crystal monochromator. Details of the optimization of this setup for low-energy studies have been described previously.[35] Data were measured at room temperature by fluorescence using a Lytle detector. All samples were run as solids, which were ground finely and dispersed as thinly as possible on Mylar tape to minimize the possibility of self-absorption effects. Compound **2a** was measured as a solution in DCM at ~2 mM concentration at room temperature. To check for reproducibility, two to three scans were measured for each sample. The energy was calibrated from sulfur K-edge spectra of $Na_2S_2O_3 \cdot 5H_2O$, run at intervals between sample scans. The maximum of the first pre-edge feature in the spectrum was fixed at 2472.02 eV. A step size of 0.08 eV was used over the edge region. Data were averaged, and a smooth background was removed from all spectra by fitting a polynomial to the pre-edge region and subtracting this polynomial from the entire spectrum. Normalization of the data was accomplished by fitting a flattened polynomial or straight line to the postedge region (2490−2635 eV) and normalizing the postedge to 1.0.

Materials. The ligand 1,2-bis(4-*tert*-butylphenyl)-ethylene-1,2-dithiolate(2−) (B) and the complex $[Pt^{II}(B^{\bullet})_2]$ have been prepared as described in the literature.[30] K_2PtCl_4, ferrocenium hexafluorophosphate, and ^{t}bpy were commercially available and were used as received without further purification.

Synthesis of the Ligand A. 1,2-Bis(isopropylthio)benzene (1 g, 4.4 mmol) in 5 mL of *n*-hexane was added dropwise to a stirred mixture of *n*-buthyllithium (1.04 g, 22 mmol) and 5 equiv of *N*,*N*,*N*′,*N*′-tetramethylenediamine (2.56 g, 22 mmol) at −50 °C. The cold bath was immediately removed, and 6 equiv (2.87 g, 26.4 mmol) of chlorotrimethylsilane was added. After 5 h of stirring at 25 °C, the solution was treated with 50% aqueous HCl (30 mL). The reaction mixture was extracted with *n*-hexane, dried over Na_2SO_4, and concentrated under reduced pressure. This step yields 1.22 g (93%) of 1,2-bis(isopropylthio)-3-trimethylsilylbenzene as a yellow oil and a small amount of the disubstituted compound. The above procedure was repeated by using the crude oily product of the first step. Yield: 1.39 g (92%).

1,2-Bis(isopropylthio)-3,6-bis(trimethylsilyl)benzene. The white solid was recrystallized from a minimal amount of *n*-hexane at 5 °C. GC−MS: m/z = 370, 255 $[M]^+$. Anal. Calcd for $C_{18}H_{34}S_2Si_2$: C, 58.3; H, 9.2; S, 17.3; Si, 15.2. Found: C, 58.6; H, 9.5; S, 17.0; Si, 15.2. ^{1}H NMR ($CDCl_3$, 400 MHz, 300 K): δ = 0.34 (s, 18H), 1.12 (d, 12H), 3.95 (sept, 2H), 7.34 (s, 2H). ^{13}C ($CDCl_3$, 100 MHz, 300 K): δ = 1.1, 22.7, 38.6, 133.5, 146.4, 149.2. The protecting isopropyl groups were removed via reduction with NH_3/Na as described in the literature.[29]

$[Pt^{II}(^t bpy)(A)]$ (1). To an acetonitrile solution (20 mL) of $[Pt^{II}(^t bpy)Cl_2]$ (0.200 g, 0.37 mmol) Na_2A (0.122 g, 0.37 mmol) in methanol (10 mL) was added dropwise. The color changed immediately to deep purple. After 3 h of stirring, the solution was concentrated under vacuum and cooled to 5 °C. Suitable crystals for X-ray diffraction analysis were obtained after 3 days. EIMS (in CH_2Cl_2): m/z 782 $[M]^+$. Anal. Calcd for $C_{30}H_{44}N_2S_2Si_2Pt$: C, 48.2; H, 5.7; N, 3.7. Found: C, 48.5; H, 5.6; N, 3.8. ^{1}H NMR ($CDCl_3$, 400 MHz, 300 K): δ = 0.48 (s, 18H), 1.42 (s, 18H), 6.95 (s, 2H), 7.52 (quart, 2H), 7.89 (s, 2H), 9.25 (d, 2H).

$[Pt^{II}(^t bpy)(B)]$ (2). To a 40 mL acetone/water (15:1) suspension of $[Pt^{II}(^t bpy)Cl_2]$ (0.380 g, 0.71 mmol) a cold dioxane solution of the ligand thiophosphoric ester[30] was added (~0.6 mmol/mL, 1.2 mL). The reaction mixture was refluxed at 65 °C for 4 h under argon while its color changed from yellow to greenish-blue. The precipitated product was filtered off and washed with a high amount of methanol and some toluene. It was dried on the filter and washed with CH_2Cl_2. The solution was evaporated to give **2** as a blue crystalline product. Yield: 0.15 g (24%). ESIMS (positive ion mode in CH_2Cl_2): m/z = 817.4 $[M]^+$. Anal. Calcd for $C_{40}H_{50}N_2S_2Pt \cdot 0.25CH_2Cl_2$: C, 57.6; H, 6.0; N, 3.3. Found: C, 57.6; H, 6.0; N, 3.1. ^{1}H NMR ($CDCl_3$, 400 MHz, 300 K): δ = 1.28 (s, 18H), 1.42 (s, 18H), 7.24 (s, 4H), 7.46 (s, 4H), 7.58 (d, 2H), 7.83 (s, 2H), 9.25 (s, 2H).

$[Pt^{II}_2(^t bpy)_2(B^{\bullet})_2](PF_6)_2$ (2c). Ferrocenium hexafluorophosphate (0.0198 g, 0.06 mmol) was dissolved in CH_2Cl_2 (40 mL) under argon, and **2** (0.0490 g, 0.06 mmol) was added. The mixture was stirred for 30 min at room temperature. The solvent was evaporated, and the solid residue was washed with *n*-pentane several times. Compound **2c** gave suitable crystals for X-ray analysis by recrystallization from CH_2Cl_2 by layering *n*-hexane on the solution. Yield: 0.045 g (75%). ESIMS (positive and negative ion mode in CH_2Cl_2): m/z 817.5 $[M]^+$, 144.8 $[PF_6]^-$. Anal. Calcd for $C_{80}H_{100}N_4S_4F_{12}P_2Pt_2$: C, 49.9; H, 5.2; N, 2.9. Found: C, 50.3; H, 5.2; N, 2.8.

Synthesis of $[Pt^{II}(PPh_3)_2(B)]$ (3). This compound was synthesized according to the literature method[31] starting with $[Pt^{II}(B^{\bullet})_2]$ (0.160 g, 0.18 mmol) and 0.950 g (3.6 mmol) of PPh_3. The product was recrystallized from a $CHCl_3$/EtOH mixture. Yield: 0.153 g (80%). ESIMS (positive ion mode in CH_2Cl_2): m/z = 1074.3 $[M]^+$, 1096 $[M] + Na^+$. Anal. Calcd for $C_{58}H_{56}P_2S_2Pt$: C, 64.9; H, 5.3. Found: C, 65.0; H, 5.3. ^{1}H NMR ($CDCl_3$, 400 MHz, 300 K): δ = 1.18 (s, 18H), 6.95 (dd, 6H), 7.12 (t, 12H), 7.24 (dd, 8H), 7.50 (m, 12H).

Acknowledgment. We thank the Fonds der Chemischen Industrie for financial support. SSRL operations are funded by the Department of Energy, Office of Basic Energy Sciences. The Structural Molecular Biology program is suported by the National Institutes of Health, National Center for Research Resources, Biomedical Technology Program and by the Department of Energy, Office of Biological and Environmental Research.

Supporting Information Available: X-ray crystallographic files in CIF format of **1**, **2c**, **3**, and **4**. This material is available free of charge via the Internet at http://pubs.acs.org.

IC070130+

(35) *ShelXTL*, version 5; Siemens Analytical X-Ray Instruments, Inc.: Madison, WI, 1994.
(36) Sheldrick, G.M. *ShelXL97*; University of Göttingen: Göttingen, Germany, 1997.
(37) Hedman, B.; Frank, P.; Gheller, S. F.; Roe, A. L.; Newton, W. E.; Hodgson, K. O. *J. Am. Chem. Soc.* **1988**, *110*, 3798−3805.